SIGNAL PROPAGATION IN AQUACULTURE ENVIRONMENT FOR WIRELESS SENSOR NETWORK APPLICATIONS

A. Harun[1], D. L. Ndzi[2, *], M. F. Ramli[1], A. Y. M. Shakaff[1], M. N. Ahmad[1], L. M. Kamarudin[1], A. Zakaria[1], and Y. Yang[2]

[1]School of Mechatronic Engineering, University of Malaysia Perlis, Perlis, Malaysia

[2]School of Engineering, University of Portsmouth, Portsmouth PO1 3DJ, UK

Abstract—This paper presents results of signal propagation studies for wireless sensor network planning in aquaculture environment for water quality and changes in water characteristics monitoring. Some water pollutants can cause widespread damage to marine life within a very short time period and thus wireless sensor network reliability is more critical than in crop farming. This paper shows that network coverage models and assumptions over land do not readily apply in tropical aquaculture environment where high temperatures are experienced during the day. More specifically, due to high humidity caused by evaporation, network coverage at 15 cm antenna height is better than at 5 m antenna heights due to the presence of a super-refraction (ducting) layer. For a 69 m link, the difference between the signal strength measured over several days is more than 7 dBm except under anomaly conditions. In this environment, the two-ray model has been found to provide high accuracy for signal propagation over water where there are no objects in close proximity to the propagation path. However, with vegetation in close proximity, accurate signal variation predication must consider contributions from scattered and diffused components, taking into account frequency selective fading characteristics to represent the temporal and spatial signal variations.

1. INTRODUCTION

Wireless sensor network (WSN) devices are now widely used for environmental monitoring and in agriculture, especially as they allow conditions to be monitored continuously on a remote basis. Because of the diversity of the scenarios where WSNs are used, most research activities have focused on improving the network architecture, accuracy, efficiency and operations [1–5]. On land, signal propagation is influenced by a large number of factors that range from static objects, e.g., trees and terrain, to mobile objects such as motor vehicles. On water, such objects are seldom present and variations are induced by changes in the atmospheric conditions above the water surface, especially for links with low antenna heights.

Intensive aquaculture is seen as the solution to the high demands for fish and seafood amidst declining sea and ocean fish stocks. Unlike in crops or animal farming on land, fish is highly susceptible to pollutants in water as it ingests water as part of the respiratory process. In addition, some species are highly sensitive to low dissolved oxygen in water, temperature, salinity and pH level of the water. Most aquaculture farms are located near rivers or streams, many of which run through farmlands where fertilizers are widely used. Wash-off from these farms lead to nitrate in the water which may contaminates fish stocks in the rivers or farms along the river. Therefore, the deployment of sensors is not only important to monitor water quality but it could be used to provide early warning of contaminants in the water and also to monitor fish stocks. Recent increase in incidences of mass shrimp mortality rate in seafood farms in Asia, for which the cause has not yet been identified, has resulted in calls for wireless sensor networks deployments for multi-modality water condition monitoring as part of an effort to identify the causes [6] and assess the impact of climate change on aquaculture, in general [7].

Many other new applications have also emerged for WSN [8–14]. The key challenges in WSN deployment is in optimizing power consumption, maintaining connectivity and reducing interference. The standard for short range wireless communication has made the implementation of WSN systems, co-existence with other wireless devices and, interoperability, much easier. However achieving optimum performance and minimizing cost in a wide area WSN deployment is still a major challenge [15]. Optimal propagation is an important requirement in order to maintain connectivity and a good quality of service. Because of the low transmission power of wireless sensor devices, three states of connectivity have been identified: connected, transitional, and disconnected [16]. The study in [17] showed that in

a high density WSN network, close to 50% of the nodes can be in the transitional state which is unreliable leading to communication errors. This transition state is mainly characterized by packet loss. Although range can be extended through the application of directional or smart antennas, they limit the flexibility of the network and the circuitries employed in some smart antennas lead to more power consumption by the nodes [18]. In general, channel measurements are often augmented with modeling and simulations to provide a wider assessment of system performances for different configurations in different scenarios [19–21].

This paper is organized as follows: Section 2 describes some of the models used in radio wave propagation that are relevant to this study. Section 3 presents the system and the measurements conducted in this study. Section 4 presents the results and the inferences that have been drawn whilst Section 5 presents the modeling that has been conducted. Conclusions are drawn in Section 6.

2. RADIO WAVE PROPAGATION

Radio waves propagation is influenced by the refractive index of the medium (air) through which it is transmitted. The refractive index, n, of air is very close to unity. Therefore refractivity, N, is normally used to describe the spatial and temporal variations of atmospheric refractive index [22] and is computed as follows:

$$N = (n - 1) \cdot 10^6 \quad (N \; units) \tag{1}$$

The refractive index can be measured using refractometer or computed from the temperature, $T(K)$, pressure, $P(mb)$, and relative humidity, $H(\%)$, measurements. Refractivity is calculated using [23]

$$N = 77.6 \frac{P}{T} + 3.732 x 10^5 \frac{e}{T^2} \quad (N \; units) \tag{2}$$

where e is the water vapour pressure given by

$$e = 0.0611 \cdot H * \exp \left(19.7 \frac{T - 273.5}{T} \right) \quad (mb) \tag{3}$$

A number of authors have put forward different coefficient values for Equation (2) [24, 25]. For increasing height, N is normally expected to decrease. However, within short height separations, the variation in humidity and airflow can be sufficiently significant to result in stratified refractivity structure of the air. This is a likely scenario in an aqua environment in tropical climate where high temperatures may lead to saturation of the air layer immediately above the water surface which may decrease rapidly with height. The impact

of this micro-scale variation is the possibility of different network performances at different antenna heights. Refractivity variations over small heights have somewhat been neglected as most studies focus on variations over hundreds of meters or several kilometers. However, the wide applications of short range radio networks, such as sensor networks, imply that these small changes are critical to the effective implementation of WSN over large areas.

   In most instances, at least two signal components propagate from the transmitter through different paths and experience different attenuation levels to the receiver. Ground reflected signal is often present for most WSN deployments in fields, depending on the antenna heights and the distance between the antennas. In general, the received signal (P_r) can be computed using

$$P_r = \frac{P_t G_t G_r \lambda^2}{(4\pi)^2 d^2} \cdot \left| 1 + \alpha_1 e^{j\psi_1} + \alpha_2 e^{j\psi_2} + \eta \right|^2 \qquad (4)$$

where P_t is the transmitted power, d is the distance, λ is the radio wavelength and, G_t and G_r are the transmitter and receiver antenna gains, respectively. The parameters α_1 and φ_1 are the reflection coefficient and phase difference between the direct wave and the reflected wave [10]. α_2 and φ_2 represent the general amplitude factor and phase difference compared to the direct ray of any component that could be received either due to reflection, diffraction or scattering from other objects and η is the term due to the effect of surface waves. Considering the first two terms in the bracket, the path length dependent phase difference between the direct and ground reflected paths is given by

$$\psi_1 = \frac{2\pi d}{\lambda} \left\{ \sqrt{\left(\frac{h_t + h_r}{d} \right)^2 + 1} - \sqrt{\left(\frac{h_t - h_r}{d} \right)^2 + 1} \right\} \qquad (5)$$

where h_t and h_r are the transmitter and receiver antenna heights, respectively. For large antenna separation where d is much larger than h_t and h_r, the phase difference can be approximated by

$$\psi_1 \approx \frac{4\pi h_t h_r}{\lambda d} \qquad (6)$$

Assuming perfect reflection $\alpha_1 = -1$ and $\varphi_1 \ll 1$ then $\alpha_1 e^{j\varphi_1} = -1 - j\varphi_1$. Using these, the direct and reflected components of Equation (4) combine to form the plane earth model which is given by

$$P_r' = \frac{P_t G_t G_r h_t^2 h_r^2}{d^4} \quad (W) \qquad (7)$$

From Equation (7), doubling the transmitter or receiver antenna height increases the received signal power by $6\,\mathrm{dBm}$ [26]. Since surface waves decrease rapidly with distance, η can reasonably be assumed to be zero. Therefore combining Equations (4) and (7) gives

$$P_r = \frac{P_t G_t G_r \lambda^2}{(4\pi)^2 d^2} \cdot \left| \frac{h_t^2 h_r^2}{d^2} + \alpha_2 e^{j\psi_2} \right| \tag{8}$$

The term $\alpha_2 e^{j\varphi_2}$ allows single or congruent effects due to multipath propagation to be incorporated into the model.

Ground reflection is present when the boundary of the first Fresnel Zone, h_0, is equal to or greater than, the antenna height [27, 28].

$$h_0 = \frac{1}{2}\sqrt{\lambda d} \quad (m) \tag{9}$$

For antennas close to the ground or for high frequencies, the distance is shorter than for high antennas and low frequencies.

ZigBee devices have a number of frequency components within the bandwidth and therefore would suffer from frequency selective fading. The measured signal strength can be represented by

$$P_r = \sum_k^N \sum_{i=0}^M \alpha_i e^{-j(\omega_0 + k\omega_s - \beta_i)\tau_i} \tag{10}$$

where N is the number of frequency components within the bandwidth, M is the number of multipath components, $\omega_0 = 2\pi f_0$ is the fundamental frequency within each channel and ω_s is the separation between the frequency components within the bandwidth. The parameters $\alpha_i e^{j\beta_i}$ and τ_i are the amplitude and time delay of each component with $\tau_0 = 0$ for the direct path and $\alpha_0 e^{j\beta_0}$ is equal to the power of the direct ray, assuming free space propagation.

3. EXPERIMENTAL SYSTEM AND SETUP

These studies were conducted in Perlis, the northernmost state in Malaysia at the border with Thailand. This region has a micro-climate that is characterized by comparatively dry months between December and March. The highest temperature in Malaysia has been recorded in this region. It has a generally flat topology with rice fields that are flooded in pre-planting periods.

Figure 1 shows a MEMSIC Solutions WSN node (model: IRIS) [29]. It consists of a communication module that uses the Atmel RF230 radio transceiver that implements the IEEE802.15.4 (ZigBee) standard [30]. The transceiver communicates in the frequency range
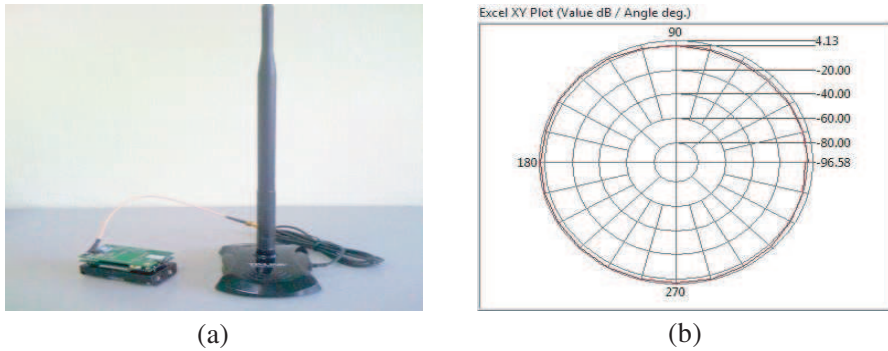
Figure 1. (a) MEMSIC wireless sensor mote which has an integrated temperature and humidity sensor, (b) measured antenna radiation pattern.

2.405–2.48 GHz and was configured to transmit data at a power setting of 3 dBm every 3 s. There are 16 channels within this ZigBee band with centre frequencies that are separated by 5 MHz and each channel has a signal bandwidth of 2 MHz.

The RF receiver sensitivity is rated at −91 dBm. The motes that were used in this study each has three onboard sensors; temperature, humidity and barometric pressure sensors. The transceivers also measure the radio signal strength indicator (RSSI) which can be used as signal level indicator. Although this may not be absolutely precise, it gives a relative reading that can be normalized to a reference distance. This is sufficient for propagation studies where the interest is in the path loss profile. The nodes were fitted with 4.13 dBi omni-directional antennas. Since no further modifications of the hardware were carried out, interested readers are referred to [29] for technical details of the IRIS motes. An image of one of the nodes and the measured antenna radiation pattern are shown in Figure 1.

During measurements, the receiving node remained fixed and the transmitting node was place in different positions along a straight path as illustrated by the transmission path arrows in Figure 2. In this part of the study, the objective was to assess the channel characteristics from a sensor node to the base station. The study was conducted in an aquaculture farm that has a number of fish ponds with the largest pond having dimensions of 69 m by 27 m. The rest of the fish ponds have dimensions of 63 m by 22 m with rows of mango and coconut trees growing in-between the ponds and along the sides as illustrated in Figure 2. The ponds have different species of fish but the dominant specie is carp fish.
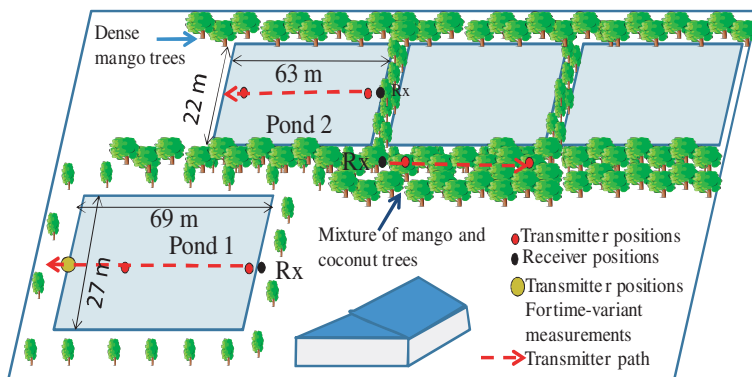
Figure 2. Measurement environment.

To evaluate signal variations with meteorological conditions, a study was conducted with wireless sensor nodes links across Pond 1 with simultaneous measurements at 15 cm and 5 m antenna heights. The nodes at 5 m height were mounted on masts and all nodes were shielded from direct sunlight. The measured parameters included the signal strength, barometric pressure, temperature and humidity. Data was collected continuously over a number of days.

4. MEASUREMENT RESULTS

Figure 3 shows the signal variation with distance over the ponds and vegetation along the sides. It can be seen that the signal variation across Pond 1 (largest pond) is smooth and fairly consistent with distance until towards the end. Results from Pond 2 (smaller pond) show more spatial signal variations. This can be explained by the close proximity of vegetation to the measurement path. In addition to the vegetation being further from the measurement path in Pond 1, it was sparsely planted. Scattered signal from the vegetation into the receiver influences the received signal depending on the relative delay and amplitude.

Measurement results along two vegetation paths with different densities show that with vegetation in the propagation path, excess vegetation attenuation introduces more than 10 m reduction in the wireless sensor node range. When compared to over the pond, there is at least 6 dB margin between receiver sensitivity level of −91 dBm and the received signal level at 69 m.

Figure 4 shows the humidity, pressure, temperature and computed refractivity of the air at 15 cm and 5 m antenna heights at Pond 1
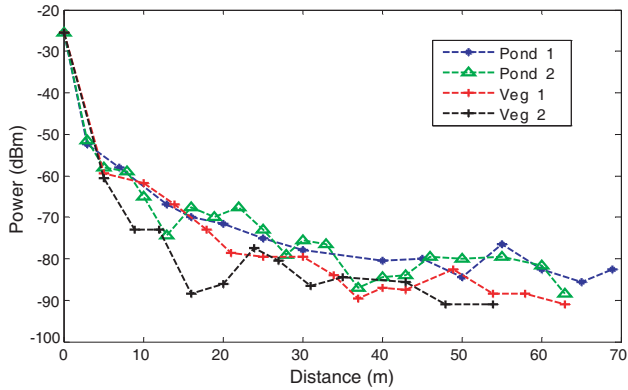
Figure 3. Comparison of signal power variation with distance over two ponds and along vegetations on the side of the ponds.

over two selected 24 hour periods. The corresponding signal variations are shown in Figure 5. Measurement in the left column of Figure 4 was conducted in dry conditions. However, for results presented in column 2, it rained from approximately 1:50 PM to 2:30 PM which resulted in a sharp drop in temperature and increase in humidity. In general, the results show that the most turbulent atmospheric conditions period is between 9:30 AM and 7:30 PM induced by the rise in temperature. From Figure 5, which shows the signal variations for the two day period, it can be seen that the system at 5 m was operating at the limit of the receiver sensitivity, with a signal to noise ratio of almost zero.

During the measurements for which results are presented in Figure 4 there was very little wind. At approximately 9 AM, the temperature rose reaching maximum at around 2 PM. In the early morning, the atmospheric pressure and humidity were high. This is matched by the low temperatures in the morning. As the temperature rises, the atmospheric pressure and humidity decrease show correlation between the measurements at both heights. At approximately 10:00, although the variations exhibit similar trends, there is a cross over between the atmospheric pressure and humidity curves from the two heights.

When the temperature increases, it increases the saturation point, i.e., increases the moisture holding capacity of the air. The heating of the water surface causes evaporation leading to higher humidity at the lower antenna height. This trend, in dry conditions, is maintained until approximately 8:30 PM. When the temperature starts to fall around 4:20 PM, humidity level starts to rise until the humidity at the lower

antenna height becomes less than that at the higher height. This rise in humidity is mainly due to a reduction in the water holding capacity of the air. Rain changes this trend, as shown in the right column in Figure 4 for Day 2, and the impact on atmospheric pressure affects the higher antenna height more than the lower one.

The calculated refractivity lies between 365 and 408 N units, which is higher than the values reported in most literature for atmospheric refractivity profiles. The proximity to water and the high temperatures combine to produce these high values.
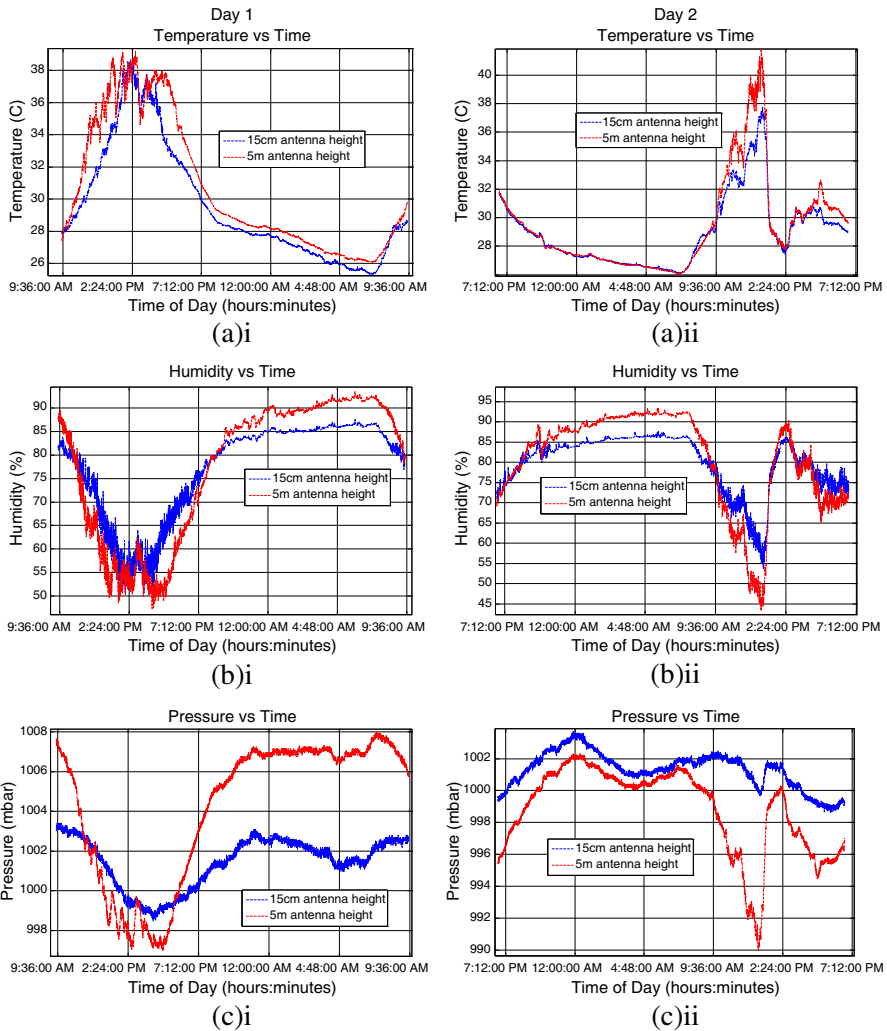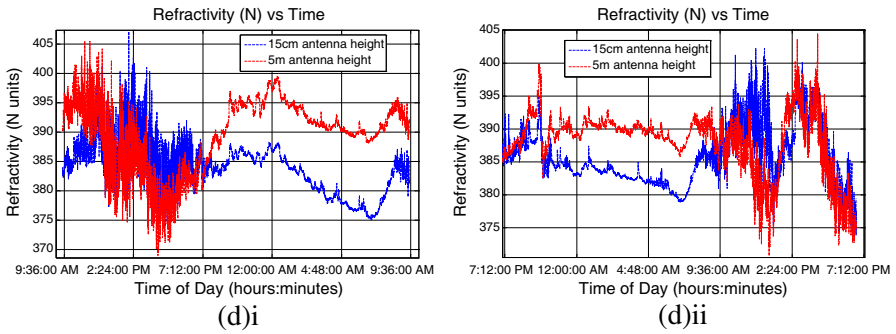
Figure 4. Variation of atmospheric conditions with time at 15 cm and 5 m antenna heights (a) temperature, (b) humidity, (c) pressure and (d) computed refractivity (N), over 24 hours periods.
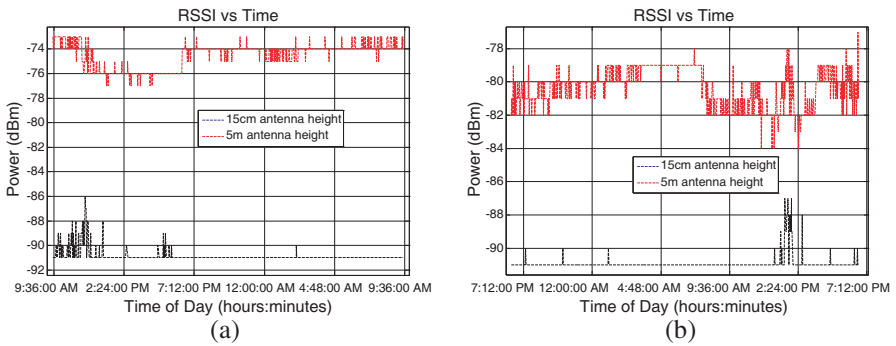

Figure 5. Variation of received signal power at 69 m antenna separation at 15 cm and 5 m antenna heights measurements. (a) Day 1, (b) Day 2.

From Figure 5(a), the average received signals power at 15 cm antenna height is -74.5 dBm compared to -90.2 dBm at 5 m height. The signal levels are quantized in 1 dBm bins. Figure 5(a) shows that the variations around noon results in spikes of signal levels that are up to 5 dBm stronger than values obtained for most of the time for 5 m antenna height. These strong signals have been recorded at 5 m antenna height when the difference in refractivity between the two heights is approximately the same (at the humidity and atmospheric pressure curves cross over points). The high signal strength at 15 cm antenna height could be attributed to either strong surface waves due to ducting-like conditions or surface reflection from the water

or both. The close proximity of the antenna to the water surface reduces the path length difference between the direct and reflected signals. Evaporation due to high temperatures during the day results in a more dispersive signal propagation medium. Recent studies in [31, 32] have shown that the formation of Somerfelt and Brillouin precursors in dispersive media lead to propagating wideband signals undergoing algebraic, rather than exponential, decay with distance. This contributes to enhanced signals arriving at the receiver. The system used in this study did not, however, have the resolution necessary to ascertain the presence of precursors. Whilst the results presented in Figure 4 were obtained for most of the time, anomalies also occur, especially after several days of dry hot conditions.

An example of received signal power over a 10 hour period (8:32 AM to 6:34 PM) when the signal levels at the two heights were close is presented in Figure 6. Figure 6(a) shows that although there were significant variations in the refractivity at the lower antenna height, the variations at 5 m was comparatively small. The probability of receiving signal levels of −83 dBm or smaller is 0.42 for 5 m antenna height compared to 0.27 at 15 cm antenna height. However, the probability of receiving signal levels of −82 dBm is almost the same at 0.72 and 0.717 at 15 cm and 5 m antenna heights. The mean values are −82.3 and −83.3, respectively. Compared to the results presented in Figure 4, only a limited data set was captured of the anomaly conditions. A long term measurement campaign is necessary for a detailed study of this type of event.

The signal strength values at 5 m dropped from 8:40 until about 10:30. After 10:48, despite greater variations in temperature, the recorded RSSI variations are over a small range. For 15 cm antenna height, the signal variations are mainly confined to a 7 dB range except for 3 instances. The drop in signal strength around 9:50 has also been reported for studies over sea paths [33], where the heat from the morning sun destroys the stratified refractive index layers in the atmosphere creating a more homogeneous air mixture. Because of the dry conditions that existed during the measurements for which the results are presented in Figure 6, this was short-lived. Evaporation creates evaporation ducts which act as a super-refraction layer that can channel the radio signals. Globally, evaporation ducts vary in height to approximately 13 m above the sea level, depending on the prevailing climatic conditions.

Correlation analyses between the different parameters have been carried out to assess their inter-dependencies. The linear cross
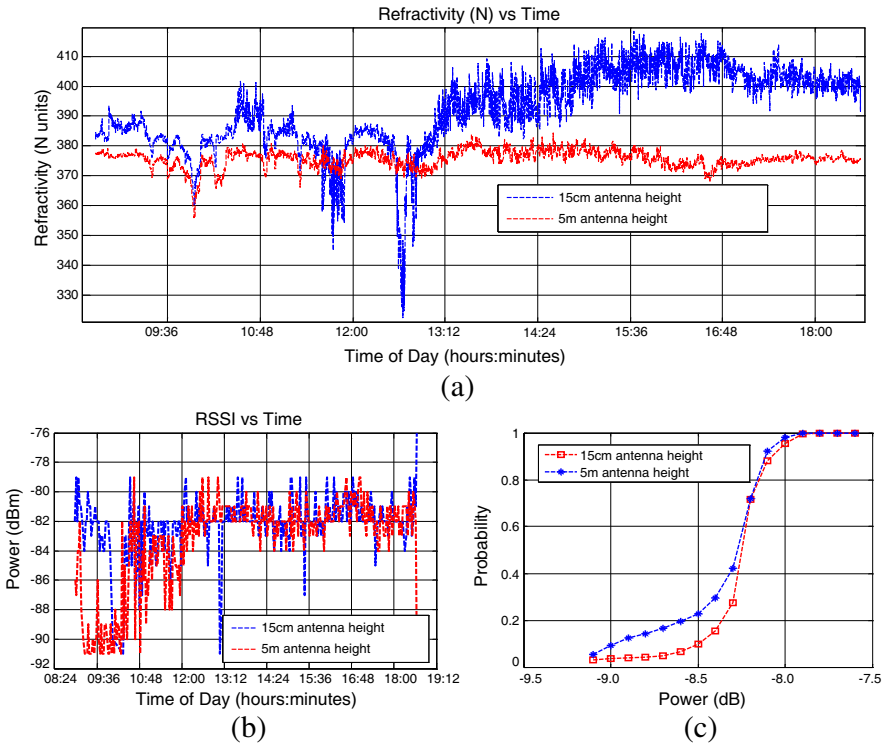
Figure 6. Anomaly: (a) refractivity, (b) signal levels and, (c) cumulative distribution of received signal power, at 15 cm and 5 m antenna heights during anomalous conditions.

correlation coefficient, r, between parameters x and y is defined by

$$r = \frac{n \sum xy - (\sum x)(\sum y)}{\sqrt{n(\sum x^2) - (\sum x)^2}\sqrt{n(\sum y^2) - (\sum y)^2}} \tag{11}$$

Using this equation, the cross correlation coefficients between the various parameters are given in Table 1. The dependency of the atmospheric pressure on temperature is revealed by the equality of their correlation coefficient values.

Differences in the refractivity between the two heights results in weak correlation between the signal levels measured at the two heights. For measurements on Day 1 (left column of Figure 4) the signal variations are independent. This could be explained by the greater differences between the conditions at the two heights.

Table 1. Correlation coefficients between measured parameter values.

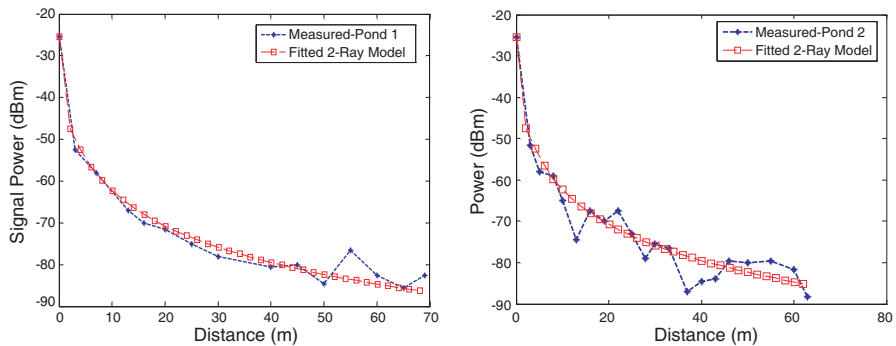| x	y	Day 1	Day 2	Anomaly
RSSI at 5 m	RSSI at 15 cm	0.044	0.429	0.301
Humidity at 5 m	Humidity at 15 cm	0.968	0.984	0.557
Temperature at 5 m	Temperature at 15 cm	0.968	0.987	0.635
Pressure at 5 m	Pressure at 15 cm	0.843	0.692	0.635

Figure 7. Measured signal level and fitted 2-ray model.

5. MODELING AND DISCUSSIONS

From Equation (9), a reflected component will be present for antenna separation of 2.8 m for the measurements across the pond. Modeling the direct signal path using free space loss model and the water reflected component, the measured and fitted model are shown in Figure 7. This uses only the first two terms of Equation (4) and no approximations of the incident angle for reflected signals have been made. For this 2-ray model, a relative permittivity, $\varepsilon_r = 81$, for fresh water is used. The root mean square error between the measured data and the fitted 2-ray model is 1.21 dB for Pond 1. This shows that a high accuracy can be achieved for system performance prediction over water. The root mean square error for Pond 2 is higher at 3.7 dB.

In Pond 1, it is reasonable to assume that only two signal paths will exist due to the low density of vegetation around the pond. In Pond 2, however, the high density of vegetation on the edges contributes significant scattered and diffused components that are strong enough to influence the received signal. Using Equation (10) and normalizing all time delay to the time of arrival of the direct components, the modeled
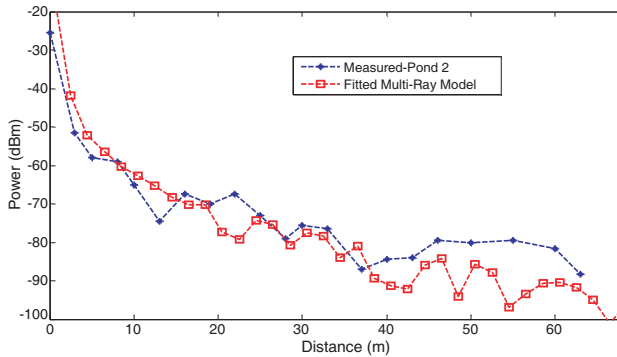
Figure 8. Multi-ray modeling of direct, reflected and tree-scattered components with path length.

received signal power across Pond 2 is shown in Figure 8. The figure only considers scattering and reflection from vegetation whose cross-section has the shortest path between the transmitter and receiver. Diffused scatter components contributions from outside this region can be judge to account for the higher average measured signal strength at large distances. This model is more realistic for the assessment of WSN performance than pure average signal strength model.

6. CONCLUSIONS

This paper has presented wireless sensor network signal propagation study in aquaculture environment in the presence of vegetation. Unlike in other forms of agriculture, water based organisms are more susceptible to changes in water quality or its constituents. Unexplained shrimp mortality, especially in Asia, has pointed to wireless sensor networks as a key technology that will enable closer monitoring of the different factors that may affect water based organisms.

Although a significant amount of studies have been conducted in WSN coverage, tropical aquaculture environment possesses unique properties. This study has shown that over large water bodies, a two ray model is sufficient for network coverage planning for antenna heights of up to 1 m. Signal variation at each position is small and variation over time is influenced by changes in temperature, humidity and hence, the refractive index of the medium. For small ponds with trees on the edges, the trees contribute to the signal variations influenced by changes in spatial variation in vegetation density and the incident, reflection and scattering angles to the transmitting and

receiving nodes. Such changes in the signal strength can be better modeled in the wideband sense by considering the frequency selective fading effects on the signal.

From the plane earth model, doubling an antenna height is equivalent to increasing the power by 6 dBm. However, this study has shown that stronger signals are received at lower antenna heights than at higher antenna heights. This can be attributed to the fact that high surface temperatures results in evaporation, thus high humidity just above the water surface. This decreases sharply with height and thus creates a super-refractive layer that channels the signal between antennas within this layer. These studies have also shown that for the same antenna separation the difference in the received signal power at 15 cm and 5 m antenna heights is at least 10 dBm. This is a critical finding for WSN deployment as this can be used, assuming no physical obstructions, to significantly enhance network coverage and/or conserve energy by using schemes such as automatic power control thereby extending the network lifetime.

REFERENCES

1. Eady, F., *Hands-on ZigBee Implementing 802.15.4 with Micro-controllers*, Newnes, Elsevier Inc., United Kingdom, 2007, ISBN: 0123708877.

2. Halgamuge, M. N., M. Zukerman, K. Ramamohanarao, and H. L. Vu, "An estimation of sensor energy consumption," *Progress In Electromagnetics Research B*, Vol. 12, 259–295, 2009.

3. Liu, H. Q., H. C. So, K. W. K. Lui, and F. K. W. Chan, "Sensor selection for target tracking in sensor networks," *Progress In Electromagnetics Research*, Vol. 95, 267–282, 2009.

4. Liu, H. Q. and H. C. So, "Target tracking with line-of-sight identification in sensor networks under unknown measurement noises," *Progress In Electromagnetics Research*, Vol. 97, 373–389, 2009.

5. Sim, Z. W., R. Shuttleworth, M. J. Alexander, and B. D. Grieve, "Compact patch antenna design for outdoor RF energy harvesting in wireless sensor networks," *Progress In Electromagnetics Research*, Vol. 105, 273–294, 2010.

6. Lightner, D. V., "Early mortality syndrome affects shrimp in Asia," *Global Aquaculture Advocate Magazine*, 40, Preferred Freezer Service, Jan. 2012.

7. Network of Aquaculture Centres in Asia-Pacific, http://www.enaca.org/modules/news/article.php?tag_id=0.

8. Nadimi, E. S., H. T. Sogaard, and T. Bak, "ZigBee-based wireless sensor networks for classifying the behaviour of a herd of animals using classification trees," *Biosystems Engineering*, Vol. 100, 167–176, 2008.

9. Nadimi, E. S., H. T. Sogaard, T. Bak, and F. W. Oudshoorn, "ZigBee-based wireless sensor networks for monitoring animal presence and pasture time in a strip of new grass," *Computers and Electronics in Agriculture*, 1–9, 2007.

10. Lee, W. C. Y., "Studies of base-station antenna height effects on mobile radio," *IEEE Transaction on Vehicular Technology*, Vol. 29, No. 2, 252–260, May 1980.

11. Lopez, M., S. Martinez, J. M. Gomez, A. Herms, L. Tort, J. Bausells, and A. Errachid, "Wireless monitoring of the pH, NH4+ and temperature in a fish farm," *Procedia Chemistry*, Vol. 1, 445–448, 2009.

12. Riquelme, J. A. L., F. Soto, J. Suardiaz, P. Sanchez, A. Iborra, and J. A. Vera, "Wireless sensor networks for precision horticulture in Southern Spain," *Computers and Electronics in Agriculture*, Vol. 68, 25–35, 2009.

13. Gay-Fernandez, J. A., M. Garcia Sanchez, I. Cuinas, A. V. Alejos, J. G. Sanchez, and J. L. Miranda-Sierra, "Propagation analysis and deployment of a wireless sensor network in a forest," *Progress In Electromagnetics Research*, Vol. 106, 121–145, 2010.

14. Mitilineos, S. A., D. M. Kyriazanos, O. E. Segou, J. N. Goufas, and S. C. A. Thomopoulos, "Indoor localisation with wireless sensor networks," *Progress In Electromagnetics Research*, Vol. 109, 441–474, 2010.

15. Verdone, R., D. Dardari, G. Mazzini, and A. Conti, *Wireless Sensor and Actuator Networks Technologies, Analysis and Design*, Academic Press, Elsevier Inc., United Kingdom, 2008.

16. Zuniga, M. and B. Krishnamachari, "Analyzing the transitional region in low power wireless links," *Proceedings of IEEE International Conference on Sensor and Ad Hoc Communications and Networks*, 517–526, 2004.

17. Ganesan, D., B. Krishnamachari, A. Woo, D. Culler, D. Estrin, and S. Wicker, "Complex behavior at scale: An experimental study of low-power wireless sensor networks," UCLA CS Technical Report UCLA/CSD-TR 02-0013, 2002.

18. Massa, A., M. Donelli, R. Azaro, and L. Fimognari, "A planar electronically reconfigurable Wi-Fi band antenna based on a parasitic microstrip structure," *IEEE Antennas and Wireless Propagation Letters*, Vol. 6, 623–626, 2007.

19. Chen, Y., Z. Zhang, L. Hu, and P. Rapajic, "Geomatry-based statistical model for radio propagation in rectangular office buildings," *Progress In Electromagnetics Research B*, Vol. 17, 187–212, 2009.

20. Chen, Y., Z. Zhang, and T. Qin, "Geomatrically based channel model for indoor radio propagation with directional antennas," *Progress In Electromagnetics Research B*, Vol. 20, 109–124, 2010.

21. Howitt, I. L. and M. S. Khan, "A mode based approach for characterizing RF propagation in conduits," *Progress In Electromagnetics Research B*, Vol. 20, 49–64, 2010.

22. Bean, B. R. and E. J. Dutton, *Radio Meteoroly*, 423, Dover Publications Inc., USA, 1996.

23. Lweis, H., "Refractivity calculations in ROPP," GRAS SAF Report 05, Met Office, UK, 2008, http://www.romsaf.org/general-documents/gsr/gsr_05.pdf, Accessed Jul. 23, 2012.

24. Mangum, J., "Atmospheric refractive signal bending and propagation delay," Report, National Radio Astronomy Observatory (NRAO), Aug. 2009, https://safe.nrao.edu/wiki/pub/Main/RefBendDelayCalc/RefBe-ndDelayCalc.pdf, Accessed Jul. 23, 2012.

25. Rüeger, J. M., "Refractive index formulae for radio waves," *Proceedings of FIG XXII International Congress*, Washington, D.C., USA, Apr. 19–26, 2002, http://www.fig.net/pub/fig_2002/js28/js28_rueger.pdf.

26. Benner, E. and A. B. Sesay, "Effect of antenna height, antenna gain, and pattern downtilting for cellular mobile radio," *IEEE Trans. on Vehicular Technology*, Vol. 45, No. 2, 217–224, 1996.

27. Ndzi, D. L., M. A. M. Arif, A. Y. M. Shakaff, M. N. Ahmad, A. Harun, L. M. Kamarudin, A. Zakaria, M. F. Ramli, and M. S. Razalli, "Signal propagation analysis for low data rate wireless sensor network applications in sport grounds and on roads," *Progress In Electromagnetics Research*, Vol. 125, 1–19, 2012.

28. Meng, Y. S., Y. H. Lee, and B. C. Ng, "Path loss modeling for near-ground VHF radio-wave propagation through forest with tree-canopy reflection effect," *Progress In Electromagnetics Research M*, Vol. 12, 131–141, 2010.

29. IRIS, MEMSIC Solution, http://www.memsic.com/products/wireless-sensor-networks/wireless-modules.html, Accessed Aug. 19, 2012.

30. Petrova, M., R. Riihijarvi, P. Mahonen, and S. Labella, "Performance study of IEEE 802.15.4 using measurements and

simulations," *IEEE Wireless Communications and Networking Conference, (WCNC 2006)*, 487–492, Las Vegas, NV, Apr. 2006.

31. Alejos, A. V. and M. Dawood, "Estimation of power extinction factor in presence of Brillouin precursors through dispersive media," *Journal of Electromagnetic Waves and Applications*, Vol. 25, No. 4, 455–465, 2011.

32. Alejos, A. V., M. Dawood, and L. Medina, "Experimental dynamical evolution of the Brillouin precursor for broadband wireless communication through vegetation," *Progress In Electromagnetics Research*, Vol. 111, 291–309, 2011.

33. Ndzi, D., J. Austin, and E. Vilar, "Wideband transhorizon channel characterization," *Radio Science*, Vol. 36, No. 5, 965–981, May 2001.